Measuring residual stress and its influence on properties of porous ZrO_2/(ZrO_2+Ni) ceramics

Wenbin Zhou[a,*] et al.

[a]*State Key Lab for Turbulence and Complex Systems, Peking University, Beijing, 100871, China*

[b]*Department of Mechanics, Beijing Jiaotong University, Beijing, 100044, China*

Abstract

Ceramic-metal functionally graded materials (FGMs) have been extensively used in aerospace engineering where high strength and excellent heat insulation materials are desired. However, their performance depends highly on the internal residual stress, which is generated inevitably due to the thermal mismatch of ceramic and metal. In this paper, based on the nanoindentation test, the field distribution of the residual stress of porous ZrO_2/(ZrO_2+Ni) ceramic-metal FGMs is measured. The residual stress field measured by nanoindentation agrees qualitatively with the finite element simulation results. Then a constitutive relation is established to investigate the effects of residual stress on the macroscopic deformation behavior of porous ZrO_2/(ZrO_2+Ni) FGMs, which agrees well with the bending and compression experiments. It is found that residual stress can improve both the flexural strength and stiffness of the porous ZrO_2/(ZrO_2+Ni) FGMs, by densifying and compensating the tensile stress of the porous middle layer (ZrO_2) during the bending process, respectively. However, it has no obvious influence on the ultimate compressive strength of the porous ZrO_2/(ZrO_2+Ni) FGMs, but mainly influences its initial stage of elastic deformation in the compressive behavior.

Keywords: Ceramic-metal functionally graded materials; Residual stresses; Nanoindentation; Finite element method

[*] Corresponding author. Tel.: +86 010 62757417
Email address: peiym@pku.edu.cn and fangdn@pku.edu.cn.

1. Introduction

Thermal Protection System (TPS) is covered on the surface of the aircraft as the thermal protecting layer. However, due to the complex shape and structure of the aircraft, a unibody design and manufacture of TPS is infeasible, therefore it is unavoidable to connect lots of thermal protection components. As a result, the thermal short problem caused by the gap between thermal protection components cannot be ignored [1]. The thermal short may lead the interior part of the fuselage structure to an extreme high temperature, severely influencing the heat insulation property of the TPS. In the process of service, the TPS has to withstand not only thermal loads, but also mechanical loads as well as harsh chemical environments, repeatedly without failure [2]. Therefore, in the study of the TPS, the analysis of the heat short effect and the use of the high temperature resistant thermal short blocking material with high strength are indispensable. Many efforts have been done on metallic thermal protection system, including the design and characterization of thermal insulation material/structure [3-8], however, the thermal short blocking material/structure has been rarely studied. Functionally graded materials (FGMs) are ideal candidates for the applications requiring multifunctional performance. For example, the ceramic-metal FGMs can be designed to take advantages of the mechanical strength of metals and the heat and corrosion resistance of ceramics [9]. Zhang et al. [10] fabricated and experimentally investigated the microstructure and thermal-mechanical properties the porous ZrO_2/(ZrO_2+Ni) ceramics and found that they had a low thermal conductivity and high strength. Therefore, the ceramic-metal FGMs can be a potential candidate for thermal short blocking materials. However, most of the FGMs have thermal residual stress due to a gradually macroscopic change in composition, and the residual stresses are destined to affect the mechanical property and service reliability of the FGMs [11-12]. So it is of great importance to understand and be able to predict the distribution and magnitude of thermal residual stress in the FGMs and multi-layer materials.

Residual stress can have both advantageous and disadvantageous effects on the performances of the FGMs. On the one hand, residual stress can be designed to enhance the fracture toughness of ceramics. Studies conducted by Blugan et al. and Bermejo et al. showed that the residual compressive stress in laminated ceramics arising from the mismatch in coefficients of thermal expansion between the different layers can enhance the fracture toughness remarkably [13-14]. On the other hand, residual stresses are not only produced within FGMs and multi-layer materials, but also in the interface between the ceramic and metal, which may cause the debonding of the layers. Based on the basic assumptions of the shear-lag theory, Nairn and Mendels [15] proposed an optimal shear-lag method for the plane stress problems of the layered material, which can give the analytical expression of the interlaminar shear stress and the residual normal stress of each layer of the multi-layer materials. Suhir [16] established the theoretical model of residual stresses in multi-layer material interface with the theory of bending stress, and the distribution formulae of stress such as shear stress, normal stress and peel stress were deduced. These models have great significance in predicting residual stress theoretically, however, they both have some ideal assumptions, which greatly limited their ranges of application. For example, Nairn assumed that the peel stress perpendicular to the interface is zero, and Suhir assumed that at least one of the multi-layer components is thick and stiff enough, so that this component and the assembly as a whole do not experience bending deformations.

Many test methods are currently available for the estimation of residual stress [17-19]: X-ray diffraction, strain/curvature measurements, hole drilling, etc. However, the widespread applications of each of these methods for most practical situations are restricted because of accuracy of measurement, spatial resolution, and applicability to a broad range of materials. X-ray diffraction is only applicable to materials that are of reasonably fine grain size, and the expensive delicate apparatus also limits its applications. The residual stress obtained by the strain/curvature measurements is the overall residual stress, and may not be applicable for coatings and FGMs, who have uneven distribution of the residual stress. Hole drilling has more widely applications, but it is necessarily destructive and cannot be directly checked by repeat measurement. Since residual stress is a key parameter that should be considered for material design and quality inspection, it is of great significance to characterize the unevenly distributed residual stress of ceramic-metal FGMs. Nanoindentation test has been widely used for measurement of local hardness and modulus of at the micro and nano scale. It has been proved that nanoindentation test data can be used for extracting specific material properties. For example, Giannakopoulos and Suresh [20] developed models to convert experimental data into material properties by considering the effect of pile-up and sink-in, as well as strain hardening. Chen et al. [21] developed models to convert nanoindentation test data into residual stress, substrate effect and creep of some homogenous bulk elastic-plastic materials. By measuring local properties, the unevenly profile of the residual stress can be obtained by nanoindentation, with high spatial resolution.

In this paper, firstly a nanoindentation experiment is conducted to study the nano mechanical property of the porous ZrO_2/(ZrO_2+Ni) ceramic-metal FGMs, which are fabricated as the thermal short blocking materials by cold isostatic pressing and pressureless sintering (CIP-PLS), and whose microstructures and properties are experimentally studied [10]. Then a method for charactering the residual stress of porous ZrO_2/(ZrO_2+Ni) ceramic-metal FGMs is adopted based on the nanoindentation test. The residual stress field measured by nanoindentation qualitatively agrees well with the finite element methods. At last, the flexural and compressive behavior of the porous ZrO_2/(ZrO_2+Ni) ceramic-metal FGMs are investigated by FEM, the effects of residual stress on the flexural behavior as well as the nonlinear compressive behavior are analyzed in detail and compared with experimental results.

2. Characterization of Residual Stress and its influence on the mechanical behavior of FGMs

2.1. Residual stress and Nanoindentation characterization

Porous ZrO_2/(ZrO_2+Ni) ceramic-metal samples of Φ8 mm (diameter)×34 mm (height) are fabricated [10], with the height of the bearing load layer (layer a, 12% porosity), transition layer (layer b, 15% porosity) and middle layer (layer c, 30% porosity) being l_a=9mm, l_b=3mm, and l_c=10mm in x direction, respectively (see Fig.1). Due to the mismatch in coefficients of thermal expansion between different layers, residual stresses are generated inevitably during the cooling process form sintering temperature to room temperature. For the dimension in axial direction is much greater than that in radial direction, and the constituents' properties vary along the axial direction, during the cooling process, the FGMs shrinks mainly in axial direction, producing unevenly distributed residual stresses. As the thermal expansion coefficient of ZrO_2 is lower than that of Ni, the middle layer c (ZrO_2) of the FGMs shrinks slower than that of the layer a and layer b, therefore, the middle layer c (ZrO_2) will be compressed, the bearing load layer a (ZrO_2+30 vol. %Ni) will be tensed, and the transition layer b (ZrO_2+15 vol. %Ni) will part be compressed (near middle layer c), part be tensed (near the bearing load layer a).

To investigate the effects of residual stress, the samples of 5mm×5mm×34mm are cut off from the as-sintered ceramics and are conducted for nanoindentation test. The selected indentation points are shown in Fig.2. The nanohardness and modulus test of the porous ZrO_2/(ZrO_2+Ni) ceramic-metal FGMs are performed on Nanomechanical Test System (TI-900 TriboIndenter, Hysitron Inc., USA) with a Berkovich tip, whose maximum indentation load and displacement are 10mN and 5 μm . The indenter is first brought into contact with the surface and the load is increased up to 10mN or 2mN (interface) in 10s at a constant load rate. The load is then hold constant for 2s and gradually decreases to zero in 10s. The Oliver-Pharr method [22] is used to calculate the reduced modulus E_r and indentation hardness H from load-displacement curves.

$$E_r = \frac{\sqrt{\pi}}{2}\frac{S}{\sqrt{A}} \quad (1)$$

$$H = \frac{F_{\max}}{A} \quad (2)$$

where S is the contact stiffness and can be determined by curve fitting the upper portion of the unloading curve and measuring its slope at peak load $S = (dF/dh)\big|_{h=h_{\max}}$, A is the projected area of the contact, and $F_{\max}$ is the maximum indentation load. The sample's modulus can be obtained using the reduced Young's modulus:

$$\frac{1}{E_r} = \frac{1-\mu^2}{E} + \frac{1-\mu_i{}^2}{E_i} \quad (3)$$

where E and μ are Young's modulus and Poisson's ratio of the sample, respectively. E_i and μ_i are Young's modulus and Poisson's ratio of the indenter probe, respectively.

Suresh and Giannakopoulos [20] developed a method by comparing the difference in contact areas of stressed and unstressed materials, when indented to the same depth. The contact areas can be measured either indirectly, by measuring the contact stiffness and relating it to the contact area through Eq. (1), or directly, by imaging the contact impression. However, due to the influences of the stress on the contact area are relatively small, this method is more appropriate to the situation where the residual stress is near the yield stress and where the pile-up within materials is appreciable. In this section, a dimensional analysis approach is used for the ceramic-metal FGMs based on the previous work of Chen [21]. Although it may have less analytical significance, the methodology can be applicable to a more complicated situation in the same way without modification and thus it has less restriction. The constitutive relation of an isotropic strain hardening material under uniaxial tension are given by

$$\sigma = \begin{cases} E\varepsilon, & \varepsilon \le Y/E \\ K\varepsilon^n, & \varepsilon \ge Y/E \end{cases}$$

(4)

To ensure continuity, the strength K can be defined by the Young's modulus E, yield strength Y, and strain hardening exponent n as

$$K = Y(E/Y)^n \quad (5)$$

The relationship between the applied load F and the penetration depth h, by dimensional analysis, can be expressed as

$$F = f(E, \nu, Y, n, h, \theta) \quad (6)$$

Applying the Π theorem in Eq. (6), we obtain:

$$\Pi_\alpha = \Pi_\alpha(\Pi_1, \nu, n, \theta) \quad (7)$$

Where $\Pi_\alpha = F/Eh^2$, $\Pi_1 = Y/E$ are dimensionless functions.

Define the effective yield strength Y^* as

$$Y^* = (YK)^{1/2} \quad (8)$$

By performing finite element analysis for a series of materials with $0 \le n < 0.5$, the relationship between F/Eh^2 and Y^*/E is found to be approximately linear and independent of n [21], which can be expressed as

$$F = Eh^2\Pi_\alpha(Y/E, n) \approx Eh^2\Pi_\alpha(Y^*/E, 0) = 5.626Eh^2(Y^*/E)^{0.5} \quad (9)$$

When there exists residual stress σ_r in the specimen, by using dimensional analysis, Eq. (9) can be rewritten as

$$F/Eh^2 = \Pi_\alpha(Y^*/E, n, \sigma_r/Y^*) = \Pi_{\alpha'}(Y^*/E) \times [1 + \Pi_\beta(Y^*/E, \sigma_r/Y^*)] \quad (10)$$

Eq. (10) is reduced to Eq. (9) when $\sigma_r = 0$, $\Pi_\beta = 0$.

By assuming a proper initial stress which represents the residual stress in the finite element model, Chen et al.[21] studied the indentation responses of 16 groups of materials with different E , Y , n , and σ_r . They found that the relationship between F / Eh^2 and σ_r / Y^* for different Y^* / E is essentially linear, the slope γ can be approximated by

$$\gamma = 19.726(Y^* / E) + 0.0182 \quad (11)$$

Substituting Eq. (9) and (11) into (10), the residual stress can be expressed as

$$\frac{\sigma_r}{Y^*} = \left[5.626(Y^* / E)^{0.5} - \frac{F}{Eh^2} \right] \Big/ \left[19.726(Y^* / E) + 0.0182 \right] \quad (12)$$

With known E , Y^* , a series of nanoindentation experiments can be performed. For each test, its F / Eh^2 value can be extracted from the corresponding $F - h$ curve. By Eq. (12), it is possible to find the residual stress. Some of the material properties used are shown in Table1 [23-26], where the specific methods for obtaining the materials properties such as Y , K can be seen in the following part B.

2.2. Finite element modeling

To verify the correctness of characterizing residual stress by indentation method, a finite element model is constructed by the commercial finite element package ABAQUS, where the specimens are assumed to be stress free at the temperature of 1200 ℃ (i.e., reference temperature), at which the sintering process is assumed to end [27]. So to all analyzed systems, the final residual stresses are only generated due to the cooling of the whole specimens from the reference temperature to room temperature (25 ℃). Here, the FE model is the same size as the experimentally tested rectangular specimen (34 mm×5 mm×5 mm, with l_a=9mm, l_b=3mm, and l_c=10mm in *x* direction). The mesh division is performed with 78,040 8-node hex elements (C3D8R). The material properties are shown in Table1, where the material constants in each composition for finite element analysis, such as Young's modulus, coefficient of thermal expansion (CTE) and Poisson's ratio, are calculated as follows [28-29]:

$$\left.\begin{aligned} E &= \frac{8E_0(1-P)(1+\mu_0)(23+8\mu_0)}{8(1+\mu_0)(23+8\mu_0)+P(5+\mu_0)(37-8\mu_0)} \\ \alpha &= \alpha_0 \quad , \quad \mu = \mu_0 \end{aligned}\right\} \quad (13)$$

where P is the porosity, E_0, α_0 and μ_0 are all dependent on the ceramic volume fraction and can be expressed from the Vegard's rule below [30]

$$M_0 = M_{ce}V_{ce} + M_m V_m \quad (14)$$

where M represents the material property parameters (E , α and μ), V_{ce} donates the ceramic volume fraction, and subscript ce and m represent ceramic and metal, respectively.

To study the influence of residual stress on the mechanical performances of the porous ZrO_2/(ZrO_2+Ni) ceramic-metal FGMs and compare with the experimental results [10], firstly we compute the residual stress of the experimentally tested rectangular specimen (34 mm×3 mm×4 mm, with l_a=8mm, l_b=4mm, and l_c=10mm in x direction), which is slightly different from our nanoindentation experimental specimen. Then we continue to simulate the three-point bending and compressive process with the existing of the residual stress. The bending process is assumed to be pure elastic with a 30 mm span, which is the same as that in our previous work [10]. Considering the plastic yielding of the Ni metal phase and the porous properties of the ZrO_2/(ZrO_2+Ni) ceramic-metal FGMs, the compressive process is assumed to exhibit the three regions: (I) elastic region characterized by elastic modulus; (II) stress plateau region characterized by a shallow slope corresponding to the plastic yielding of the Ni metal phase; and (III) densification region characterized by a relatively steep slope.

The constitutive relation of layer a and layer b is expressed as:

$$\sigma = \begin{cases} E\varepsilon, & \sigma \le Y(in\ elastic) \\ K\varepsilon^{n}, & Y \le \sigma \le \sigma_p(in\ plastic) \\ K^{'}\varepsilon^{n^{'}}, & \sigma_p \le \sigma(in\ densification) \end{cases} \quad (15)$$

where $E = E_a$, E_b is the elastic modulus of layer a and layer b, respectively. K is the strength coefficient and $0 < n < 1$ is the strain hardening exponent in each layer. Notice that in densification region, the constitutive relation is assumed to have a similar expression as that of in plastic region, but with $n^{'} > 1$. Y is the compressive yield strength before the plastic deformation of Ni and is taken to be the same as that of Ni. Considering the effect of porosity, Y can be written as [28-29]

$$Y = (1 - P)\sigma_{s0,Ni} \quad (16)$$

where P is the porosity for layer a and layer b, $\sigma_{s0,Ni} = 159MPa$ [31] is the compressive yield strength (0.2% offset) of pure dense Ni. Considering that there is no plastic for the ceramic phase, here we assume the strain hardening exponent during the plastic deformation stage is the same as that of Ni, i.e. $n = 0.147$ [32], then by considering the continuity between region (I) and region (II) at $\sigma = Y$, the strength coefficient can be given by

$$K = E^{n} / Y^{n-1} \quad (17)$$

Gibson and Ashby established [33] an equation to describe the relationship between the relative stress σ_p / σ_{s0} and the relative density ρ / ρ_0

$$\frac{\sigma_p}{\sigma_{s0}} = C(\frac{\rho}{\rho_0})^{q} \quad (18)$$

where σ_p is the collapse stress of the porous ceramic-metal FGMs when the densification occurs, σ_{s0} is the yield stress of the corresponding solid ceramic-metal FGMs and is taken to be $\sigma_{s0,Ni}$, ρ is the density of the porous

FGMs and ρ_0 is the density of the solid, respectively. C is a geometric constant and q is density exponent. The values of q are in the range 1.0-6.3 for porous materials with higher relative density (lower porosity) [34]. Maiti et al. [35] concluded that $C \approx 0.65$ and $q = 1.5$.

When the densification occurs, stress increases rapidly with the increasing of strain, the constitutive relation of the densification region (III) is assumed to be expressed as

$$\sigma = K^{'} \varepsilon^{n^{'}} \quad (19)$$

Given that the porosity is low, $K^{'}$ is taken to be the elastic modulus of layer a and layer b, respectively, but with $n^{'} > 1$ to reflect the densification effects. By considering the continuity between region (II) and region (III) at $\sigma = \sigma_p$, $n^{'}$ can be expressed as

$$n^{'} = [1 + \ln(K / K^{'}) / \ln(\sigma_p / K)]n \quad (20)$$

The typical stress-strain curve for porous ceramics under compression contains two stages, in the initial stage, the load increases linearly. When the load exceeds the crushing strength, the sample starts crushing and the load maintains a constant value, namely, the sample fractures completely only after experiencing a great deal of strain [36]. Costa Oliveira et al. [37] reported that as porous ceramics reach their compressive limit, parts of pores collapse, to release stress and thus generating strain, maintaining a certain amount of “plasticity”. The constitutive relation of layer c is expressed as:

$$\sigma = \begin{cases} E\varepsilon, & \sigma \le \sigma_{fc} \quad \text{(in elastic)} \\ \sigma_{fc}, & \sigma = \sigma_{fc} \quad \text{(in "plastic")} \end{cases} \quad (21)$$

where $E = E_c$ is the elastic modulus of layer c, σ_{fc} is the crushing strength and is taken to be 872MPa, which is the compressive strength of the pure porous ZrO_2 ceramics obtained by compression test in our previous work [10].

3. Results and Discussion

3.1. Nanoindentation Characterization of Residual Stress and Comparison with Simulated Results

Figure 3a-b show the nanoindentation experimental results of layer b (ZrO_2+15%Ni). The indentation points are shown in Fig.2, with local coordinates being x=0.5 mm, 1 mm, 1.5 mm, 2 mm, and 2.5 mm, respectively. We can see that both E and H vary at different locations in x direction, increasing monotonously with the variation of positions from the interface near layer a (tensile stress region) to the interface near layer c (compressive stress region). This result shows that residual stress indeed influences the response of the porous ZrO_2/(ZrO_2+Ni) ceramic-metal FGMs during indentation processes. Moreover, this result qualitatively agrees with those reported in previous investigations (for example, Oliver's [38] and Suresh's [39]), namely, the effect of compressive stress tends to increase the modulus and hardness, while the tensile stress tends to reduce it. Therefore, we can characterize the residual stress of the porous ZrO_2/(ZrO_2+Ni) ceramic-metal FGMs base on the nanoindentation test.

Figure 4 plots the corresponding residual stress profile in layer b (ZrO_2+15 vol. %Ni). We can see that the prediction by nanoindentation qualitatively agrees well with the finite element simulation result. Combing with the results in Fig.3, one can find that the maximum changes in E and H from tension state (38 MPa) to the unstressed state are 7% and 44%, respectively, compared with that of 3% and 22% for compressive state (-38 MPa) to the unstressed state. Therefore, the effects of tension are more pronounced than those of compression. These results agree with those reported in the previous investigation [38].

The nanoindentation experimental results of layer c (ZrO_2) are shown in Fig.5a-b, where the local coordinates of the indentation points are x=0.5 mm, 1 mm, 1.5 mm, 2 mm, and 3.5 mm, respectively, as shown in Fig.2. Figure 6 plots the relevant residual stress profile. We can see that the prediction by nanoindentation qualitatively agrees with the finite element simulation result. It is found that both the modulus and hardness are not constants in the same layer but vary nonmonotonously with the increase of x. This trend is in consistent with the axial residual compressive stress produced in layer c. The data clearly show that compressive stress has a great effect on the modulus and hardness of ZrO_2 ceramics, increasing in compressive stress leads to increase in E and H. The maximum increment in E and H are up to 16% and 73% compared with point 5 (x=3.5mm, -37MPa) and point 3 (x=1.5 mm, -88 MPa), respectively. Notice that the modulus of point 5 is very close to but slightly greater than the modulus used in FE in Table 1(115.43GPa, without stress effects), which also proves that computing the equivalent parameters with Eq.(13) is applicable. Compared with Fig.4, one can see that the effects of per unit residual compressive stress on E and H for pure ceramic (layer c) are greater than that of ceramic-metal mixtures (layer b). It may be concluded that residual stress influence more remarkable for ceramic over that of metal. This is yet to be further analyzed by our following experimental results.

Figure 7a-b show the nanoindentation experimental results of the interface between layer c and layer b. The indentation points selected are shown in Fig.2, where the local coordinates are y=0 mm, 0.55mm, 1.1mm, 1.65mm, and 2.2mm, respectively. Considering the weak strength of the interface, the maximum load is decreased from 10mN to 2mN, seen in Fig.7a. The axial residual stress in the interface is plotted in Fig.8. Again, the prediction by nanoindentation qualitatively agrees with the finite element simulation result. Residual stress in the interface is compressive in the center, gradually decreasing and turns to tensile stress as approaching the edge. One can see that both the modulus and hardness vary monotonously with the increase of y from the center to the edge of the interface, decreasing in compressive stress leads to a decrease in E and H. The E and H of the interface both have a decline compared with that of layer c. Also, The maximum decrements in E and H from compressive state (-50 MPa) to the unstressed state are 16% and 150%, respectively. These results show that residual stress especially the interfacial residual stress has a great effect on the mechanical properties.

Figure 9a-b illustrate the nanoindentation experimental results of layer a (ZrO_2+30 vol. %Ni), the relevant residual stress profile is plotted in Fig.10a-b. The selected indentation points are shown in Fig.2, with local coordinates being x=1 mm, 1.5 mm, 2 mm, 3.5 mm, and 5 mm, respectively. We can see that the variation trends of E and H are in consistent with the residual tensile stress, which show that tensile stress has a great effect on the hardness and modulus of ceramic-metal mixtures, increasing in tensile stress leads to decrease in E and H. The maximum increments in E and H from tension state (85 MPa) to the unstressed state are 4% and 46%, respectively. Compared with ceramic-metal mixtures with less metal content (see Fig.3 and Fig.4), one can see that as the increase of metal content, the effects of per unit residual tensile stress on E and H for ceramic-metal mixtures decrease. Therefore, residual stress (tensile stress or compressive stress) has a greater effect on ceramic than that of metal.

From above, we conclude that residual stress (tensile or compressive) induces changes in the apparent elastic modulus and indentation hardness of the ceramic-metal FGMs, which can be used to characterize the distribution of residual stress. The comparison with finite element results indicates the feasibility of the nanoindentation characterization of residual stress profile， especially for the turning points of tensile and compressive residual stresses in layer a and layer c, respectively. Further analysis with nanoindentation and FEM results, one can find that the residual stress in layer c (ZrO_2) and the interface of layer c (ZrO_2) have the greatest quantitative difference (see Fig.6 and Fig.8), this is mainly because the "yield strength" Y =872MPa used for porous ZrO_2 ceramic (see Eq.(21)) is essentially not the yield strength but the crushing strength, which is a result of the collapse of pores releasing stress and thus generating strain, maintaining a certain amount of "plasticity". For ceramic-metal mixtures, i.e. layer a (ZrO_2+30 vol. %Ni) and layer b (ZrO_2+15 vol. %Ni), the maximum relative error are 30% and 40%, respectively. Due to the lack of the experimental data of material properties such as Y , K for each layer, the methods we use to obtain the Y , K can only represent the real value approximately, which result in the quantitative difference in residual stress predicted by nanoindentation and FEM. Therefore, uniaxial tension experiments are needed to get the material properties of each layer in the future work.

3.2. Influence of Residual Stress on the Mechanical Performances

In this section, a rectangular ZrO_2/(ZrO_2+Ni) ceramic-metal specimen (34 mm×3 mm×4 mm, with l_a=8mm, l_b=4mm, and l_c=10mm in x direction) is studied, the three-point bending and compressive process with the existing of the residual stress is simulated by FEM and compared with experimental results [10] to investigate the influence of residual stress. Here, the load conditions are the same as that of our previous work [10], namely, a 30 mm span and a crosshead speed of 0.5 mm $\times$ min^{-1} for the three-point bending process, and a crosshead speed of 0.05 mm $\times$ min^{-1} for the compressive process. Figure 11 shows the flexural strength-displacement curves of the porous ZrO_2/(ZrO_2+Ni) ceramic-metal FGMs obtained by flexural test and FEM. The experimental result is the average value of the five experimental results in Fig.5b of our previous work [10]. Here, four different cases are simulated by the FEM, namely, (i) ceramic-metal FGMs without residual stress (RS) and densification (DS), (ii) ceramic-metal FGMs with only residual stress, (iii) ceramic-metal FGMs with only densification, and (iv) ceramic-metal FGMs with residual stress and densification. During the bending process, densification occurs because of the compressive stress produced in the top of the middle porous layer (ZrO_2). Here the densification is simulated by decreasing the porosity, namely, increasing the modulus from 115.43 GPa to 140 GPa. Comparing the case with RS and DS to the case without RS and DS, we find that the flexural strength and stiffness of the ceramic-metal FGMs are increased by 10% and 33% over that of later, respectively. Also, by comparing the cases with only RS and only DS to the case without RS and DS, one can see that compressive residual stress and densification can influence the flexural strength and stiffness of the porous ZrO_2/(ZrO_2+Ni) ceramic-metal FGMs, respectively. On the one hand, the residual compressive stress can compensate the tensile stress produced in the bottom of the middle layer (ZrO_2) during the bending process, therefore, improving the flexural strength of the porous ZrO_2/(ZrO_2+Ni) ceramic-metal FGMs. On the other hand, the residual compressive stress can promote the densification process of the middle porous layer (ZrO_2) during the bending process, which improves the stiffness of the porous ZrO_2/(ZrO_2+Ni) ceramic-metal FGMs.

Figure 12 shows the compressive strength-displacement curves of the porous ZrO_2/(ZrO_2+Ni) ceramic-metal FGMs obtained by compressive test and FEM. The experimental result is the average value of the five experimental results in Fig.4b of our previous work [10]. The one without axial residual stress is also plotted as comparison. We can see that the compressive strength-displacement curves of the porous ZrO_2/(ZrO_2+Ni) ceramic-metal FGMs exhibits the three regions: (I) elastic region; (II) stress plateau region; and (III) densification region. It is found that the residual stress has no obvious influence on the ultimate compressive strength of the ceramic-metal FGMs in contrast to the case without residual stress. The residual stress only produces limited influence on the strength-displacement relation in a shallow deformation range. The influence deformation ranges are (0, 0.6%) in strain, namely, the elastic region (I) and stress plateau region (II) . For the two cases without and with residual stress, the apparent Young's modulus decreases from 92.5 GPa to 34.6 GPa and the reduced amplitudes reach up about 63%. From above, we conclude that the decreased ultimate compressive strength should be attributed to the low compressive strength of Ni (159MPa) [31] compared with that of ZrO_2, while the residual stress decreases the apparent Young's modulus of the compressive strength-displacement curves and shows influence at the stage of initially elastic small deformation.

4. Conclusions

This paper provides a method for charactering the residual stress of porous ZrO_2/(ZrO_2+Ni) ceramic-metal FGMs based on the theoretical work of Chen, where the nanoindentation experimental data are used for extracting residual stress field. It is found that residual stress predicted by nanoindentation qualitatively agrees well with the finite element simulation results. Nanoindentation experimental results indicate that the residual stress (tensile or compressive) induces changes in the apparent elastic modulus and indentation hardness of the ceramic-metal FGMs, during which residual stress has a greater effect on ceramic than that of metal, and tensile stress influences pronounced than those of compression.

Influences of residual stress on mechanical performances of the porous $ZrO_2/(ZrO_2+Ni)$ ceramic-metal FGMs are investigated, the axial compressive residual stress can improve both the flexural strength and stiffness of the porous $ZrO_2/(ZrO_2+Ni)$ FGMs simultaneously. Residual stress has no obvious influence on the ultimate compressive strength of the porous $ZrO_2/(ZrO_2+Ni)$ ceramic-metal FGMs, but mainly influences the initial stage of elastic deformation in the compressive behavior of the porous $ZrO_2/(ZrO_2+Ni)$ ceramic-metal FGMs.

Acknowledgments

The authors are grateful for the support by the National Natural Science Foundation of China (Grant Nos. 11090330, and 11090331), the National Basic Research Program of China (973 Program, 2010CB8327001, 2011CB610303), and the Foundation of the Author of National Excellent Doctoral Dissertation of China (No. 201029).

References

[1] Ng, W.H., Friedmann, P.P., and Waas AM, "Thermomechanical Analysis of a Thermal Protection System with Defects and Heat Shorts", *47th AIAA/ASME/ASCE/AHS/ASC Structures, Structural Dynamics, and Materials Conference*, AIAA Paper 2006-2212, Newport, RI, May 2006.

[2] Ng, W.H., McNamara, J.J., Friedmann, P.P., and Waas, A.M, "Thermomechanical Behavior of Damaged TPS Including Hypersonic Flow Effects", *14th AIAA/AHI space planes and hypersonic systems and technologies conference*, AIAA Paper 2006-7951, Canberra, AU, Nov. 2006.

[3] Spinnler, M., Winter, E.R.F., and Viskanta, R., "Studies on High-Temperature Multilayer Thermal Insulations," *International Journal of Heat and Mass Transfer*, Vol. 47, No. 6-7, 2004, pp. 1305-1312.

doi: 10.1016/j.ijheatmasstransfer.2003.08.012

[4] Spinnler, M., Winter, E.R.F., Viskanta, R., and Sattelmayer, T., "Theoretical Studies of High-Temperature Multilayer Thermal Insulations Using Radiation Scaling," *Journal of Quantitative Spectroscopy & Radiative Transfer*, Vol. 84, No. 4, 2004, pp. 477-491.

doi:10.1016/S0022-4073(03)00264-4

[5] Kamran, D., "Thermal analysis and design of multi-layer insulation for re-entry aerodynamic heating," *35th AIAA thermophysics conference*, AIAA Paper 2001-2834, Anaheim, CA, Jun. 2001.

[6] Kondo, N., Suzuki, Y., and Ohji, T., "High-Strength Porous Silicon Nitride Fabricated by the Sinter-Forging Technique," *Journal of Materials Research*, Vol. 16, No. 1, 2001, pp. 32-34.

doi: 10.1557/Jmr.2001.0009

[7] Ortega, F.S., Sepulveda, P., and Pandolfelli, V.C., "Monomer Systems for the Gelcasting of Foams," *Journal of the European Ceramic Society*, Vol. 22, No. 9-10, 2002, pp. 1395-1401.

doi: 10.1016/S0955-2219(01)00486-1

[8] Zhang, G.J., Yang, J.F., and Ohji, T., "Fabrication of Porous Ceramics with Unidirectionally Aligned Continuous Pores," *Journal of the American Ceramic Society*, Vol. 84, No. 6, 2001, pp. 1395-1397.

[9] Hirai, T., Sasaki, M., and Niino, M., "Cvd in-Situ Ceramic Composites," *Journal of the Society of Materials Science, Japan*, Vol. 36, No. 410, 1987, pp. 1205-1211.

[10] Zhang, R., He, R., Zhou, W., Wang, Y., and Fang, D., "Design and Fabrication of Porous ZrO_2/(ZrO_2+Ni) Sandwich Ceramics with Low Thermal Conductivity and High Strength," *Materials & Design*, Vol. 62, Oct. 2014, pp. 1-6.

doi: 10.1016/j.matdes.2014.05.006

[11] Chu, C.L., Zhu, J.C., Yin, Z.D., and Lin, P.H., "Optimal Design and Fabrication of Hydroxyapatite-Ti Asymmetrical Functionally Graded Biomaterial," *Materials Science and Engineering a-Structural Materials Properties Microstructure and Processing*, Vol. 348, No. 1-2, 2003, pp. 244-250.

doi: 10.1016/S0921-5093(02)00738-4

[12] Lee, C.S., Ahn, S.H., DeJonghe, L.C., and Thomas, G., "Effect of Functionally Graded Material (FGM) Layers on the Residual Stress of Polytypoidally Joined Si_3N_4-Al_2O_3," *Materials Science and Engineering a-Structural Materials Properties Microstructure and Processing*, Vol. 434, No. 1-2, 2006, pp. 160-165.

doi: 10.1016/j.msea.2006.06.139

[13] Blugan, G., Dobedoe, R., Lugovy, M., Koebel, S., and Kuebler, J., "Si_3N_4-Tin Based Micro-Laminates with Rising R-Curve Behaviour," *Composites Part B-Engineering*, Vol. 37, No. 6, 2006, pp. 459-465.

doi: 10.1016/j.compositesb.2006.02.013

[14] Bermejo, R., Pascual, J., Lube, T., and Danzer, R., "Optimal Strength and Toughness of Al_2O_3-ZrO_2 Laminates Designed with External or Internal Compressive Layers," *Journal of the European Ceramic Society*, Vol. 28, No. 8, 2008, pp. 1575-1583.

doi: 10.1016/j.jeurceramsoc.2007.11.003

[15] Nairn, J.A., and Mendels, D.A., "On the Use of Planar Shear-Lag Methods for Stress-Transfer Analysis of Multilayered Composites," *Mechanics of Materials*, Vol. 33, No. 6, 2001, pp. 335-362.

doi: 10.1016/S0167-6636(01)00056-4

[16] Suhir, E., "Stresses in Bi-Metal Thermostats," *Journal of Applied Mechanics*, Vol. 53, No. 3, 1986, pp. 657-660.

doi: 10.1115/1.3171827

[17] Noyan, I. C., and Cohen, J. B., *Residual Stresses*, Elsevier, New York, 1985.

[18] Lu, J., and James, M. R., *Handbook of Measurement of Residual Stresses*, Fairmount Press, Lilburn, GA, 1996.

[19] ASTM E837 "Standard Test Method for Determining Residual Stresses by the Hole-Drilling Strain-Gage Method," 1994.

[20] Giannakopoulos, A.E., and Suresh, S., "Determination of Elastoplastic Properties by Instrumented Sharp Indentation," *Scripta Materialia*, Vol. 40, No. 10, 1999, pp. 1191-1198.

doi: 10.1016/S1359-6462(99)00011-1

[21] Chen, K.S., Chen, T.C., and Ou, K.S., "Development of Semi-Empirical Formulation for Extracting Materials Properties from Nanoindentation Measurements: Residual Stresses, Substrate Effect, and Creep," *Thin Solid Films*, Vol. 516, No. 8, 2008, pp. 1931-1940.

doi: 10.1016/j.tsf.2007.09.005

[22] Oliver, W.C., and Pharr, G.M., "An Improved Technique for Determining Hardness and Elastic-Modulus Using Load and Displacement Sensing Indentation Experiments," *Journal of Materials Research*, Vol. 7, No. 6, 1992, pp. 1564-1583.

doi: 10.1557/Jmr.1992.1564

[23] Fogaing, E.Y., Lorgouilloux, Y., Huger, M., and Gault, C.P., "Young's Modulus of Zirconia at High Temperature," *Journal of Materials Science*, Vol. 41, No. 22, 2006, pp. 7663-7666.

doi: 10.1007/s10853-006-0593-7

[24] Johnson, J., and Qu, J., "Effective Modulus and Coefficient of Thermal Expansion of Ni-Ysz Porous Cermets," *Journal of Power Sources*, Vol. 181, No. 1, 2008, pp. 85-92.

doi: 10.1016/j.jpowsour.2008.03.035

[25] Kollie, T.,G., "Measurement of the Thermal-Expansion Coefficient of Nickel from 300 to 1000 K and Determination of the Power-Law Constants Near the Curie Temperature," *Physical Review B*, Vol. 16, No. 11, 1977, pp. 4872-4881.

doi: 10.1103/PhysRevB.16.4872

[26] Farraro, R., and McLellan, R., "Temperature Dependence of the Young's Modulus and Shear Modulus of Pure Nickel, Platinum, and Molybdenum," *Metallurgical Transactions A*, Vol. 8, No. 10, 1977, pp. 1563-1565.

doi: 10.1007/BF02644859

[27] Kokini, K., Takeuchi, Y.R., and Choules, B.D., "Surface Thermal Cracking of Thermal Barrier Coatings Owing to Stress Relaxation: Zirconia Vs Mullite," *Surface & Coatings Technology*, Vol. 82, No. 1-2, 1996, pp. 77-82.

doi: 10.1016/0257-8972(95)02647-9

[28] Kingery, W. D., Bowen, H. K, and Uhlmann, D. R., *Introduction to Ceramics*, 2nd ed., John Wiley & Sons, New York, 1976.

[29] Kondo, R., Porous Materials, Gihoudo, Tokyo, 1986.

[30] Zhang, X.C., Xu, B.S., Wang, H.D., Jiang, Y., and Wu, Y.X., "Application of Functionally Graded Interlayer on Reducing the Residual Stress Discontinuities at Interfaces within a Plasma-Sprayed Thermal Barrier Coating," *Surface & Coatings Technology*, Vol. 201, No. 9-11, 2007, pp. 5716-5719.

doi: 10.1016/j.surfcoat.2006.07.062

[31] Special Metals Corporation, "Nickel 200&201.pdf ," URL: http://www.specialmetals.com/documents/Nickel 200 & 201.pdf.

[32] Gurao, N., Kapoor, R., and Suwas, S., "Effect of Strain Rate on Evolution of the Deformation Microstructure and Texture in Polycrystalline Copper and Nickel," *Metallurgical and Materials Transactions A*, Vol. 41, No. 11, 2010, pp. 2794-2804.

doi: 10.1007/s11661-010-0360-x

[33] Gibson, L. J. and Ashby, M. F., *Cellular solids: structure and properties*, 2nd ed., Cambridge University Press, Cambridge, 1997.

[34] Hakamada, M., Asao, Y., Kuromura, T., Chen, Y.Q., Kusuda, H., and Mabuchi, M., "Density Dependence of the Compressive Properties of Porous Copper over a Wide Density Range," *Acta Materialia*, Vol. 55, No. 7, 2007, pp. 2291-2299.

doi: 10.1016/j.actamat.2006.11.024

[35] Maiti, S.K., Gibson, L.J., Ashby, M.F., "Deformation and Energy Absorption Diagrams for Cellular Solids," *Acta Metallurgica*, Vol. 32, No. 11, 1984, pp. 1963-1975.

doi: 10.1016/0001-6160(84)90177-9

[36] Peng, H.X., Fan, Z., and Evans, J.R.G., "Factors Affecting the Microstructure of a Fine Ceramic Foam," *Ceramics International*, Vol. 26, No. 8, 2000, pp. 887-895.

doi:10.1016/S0272-8842(00)00032-8

[37] Oliveira, F.A.C., Dias, S., Vaz, M.F., and Fernandes, J.C., "Behaviour of Open-Cell Cordierite Foams under Compression," *Journal of the European Ceramic Society*, Vol. 26, No. 1–2, 2006, pp. 179-186.

doi: 10.1016/j.jeurceramsoc.2004.10.008

[38] Tsui, T.Y., Oliver, W.C., and Pharr, G.M., "Influences of Stress on the Measurement of Mechanical Properties Using Nanoindentation .1. Experimental Studies in an Aluminum Alloy," *Journal of Materials Research*, Vol. 11, No. 3, 1996, pp. 752-759.

doi: 10.1557/Jmr.1996.0091

[39] Suresh, S., and Giannakopoulos, A.E., "A New Method for Estimating Residual Stresses by Instrumented Sharp Indentation," *Acta Materialia*, Vol. 46, No. 16, 1998, pp. 5755-5767.

doi: 10.1016/S1359-6454(98)00226-2

Figures and Tables

Table 1 Material properties for porous ZrO_2/(ZrO_2+Ni) ceramic-metal FGMs

material	T (ºC)	E (GPa)	α (10^{-6}/K)	μ	K (MPa)	n	Y (MPa)	Y^* (MPa)
ZrO_2	25 600 1127	198.67 166.76 118.94	8 9.20 10.25	0.315	-	-	-	-
ZrO_2 (30% porosity)	25 600 1127	115.43 96.89 69.11	8 9.20 10.25	0.315	872	0	872	872
Ni	25 600 1127	205 176.82 127.65	12.73 17.93 22.51	0.3	455.638	0.147	159	269.159
ZrO_2+15%Ni (15% porosity)	25 600 1127	153.88 129.72 92.70	8.71 10.51 12.09	0.313	380.278	0.147	135.15	226.621
ZrO_2+30%Ni (12% porosity)	25 600 1127	163.08 138.04 98.83	9.41 11.82 13.93	0.311	395.056	0.147	139.92	235.109

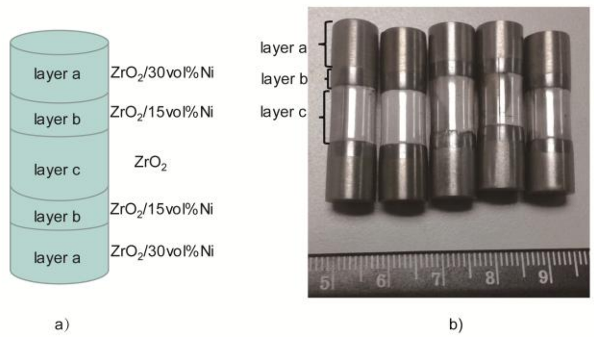

Fig.1 Schematic composition and optical photograph of the fabricated porous ZrO_2/(ZrO_2+Ni) ceramic-metal FGMs. a), b)

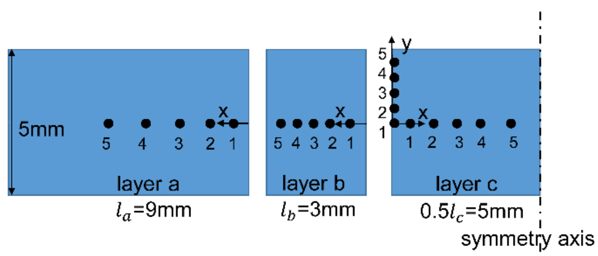

Fig.2 Illustration of the indentation points on porous ZrO_2/(ZrO_2+Ni) ceramic-metal FGMs.

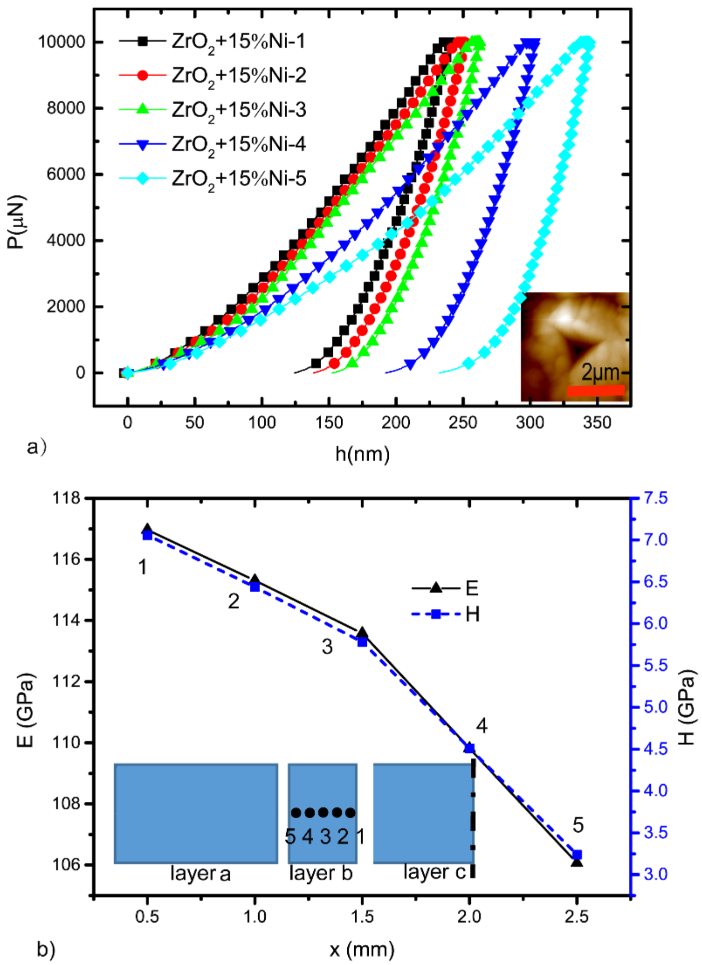

Fig.3 Nanoindentation experimental results of layer b (transition layer, ZrO_2+15 vol. %Ni): a) load-displacement curve, b) modulus and hardness

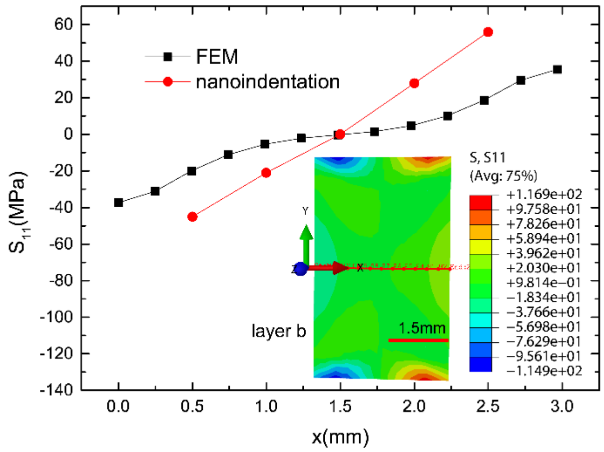

Fig.4 Comparison of residual stress of layer b determined by nanoindentation and FEM

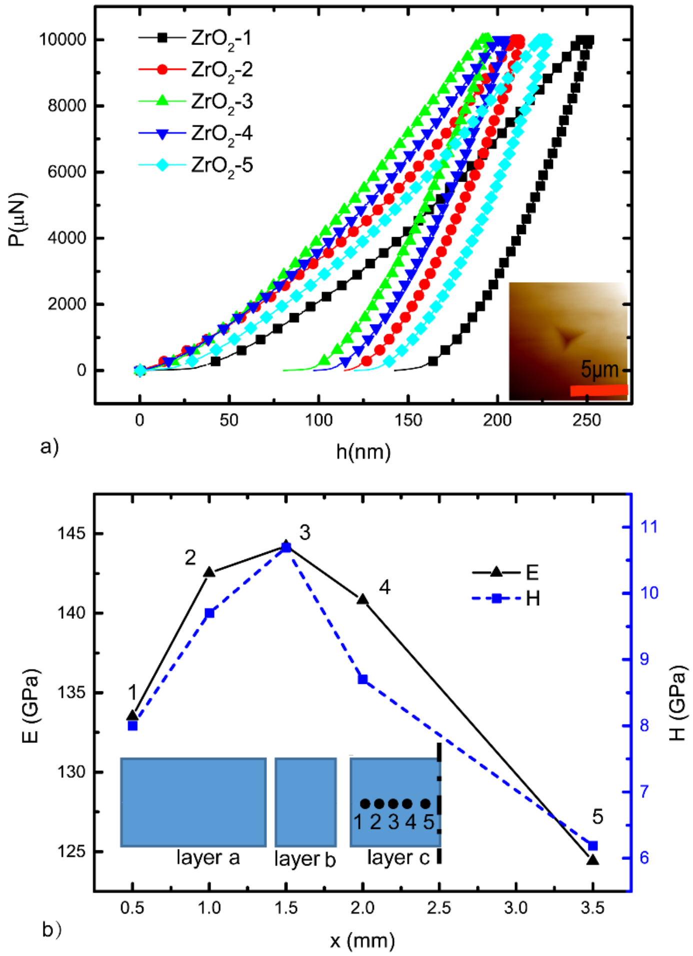

Fig.5 Nanoindentation experimental results of layer c (ZrO_2): a) load-displacement curve, b) modulus and hardness

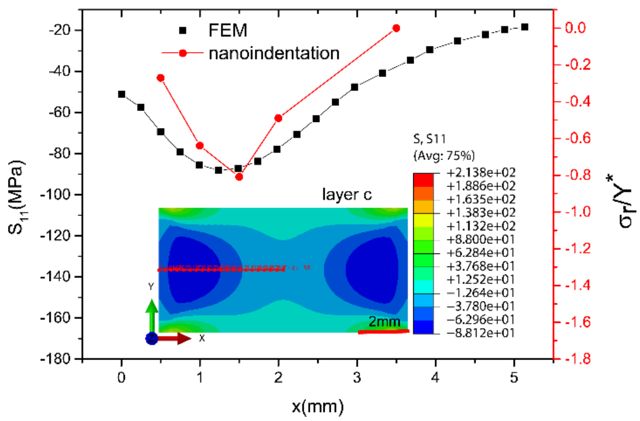

Fig.6 Comparison of residual stress of layer c determined by nanoindentation and FEM

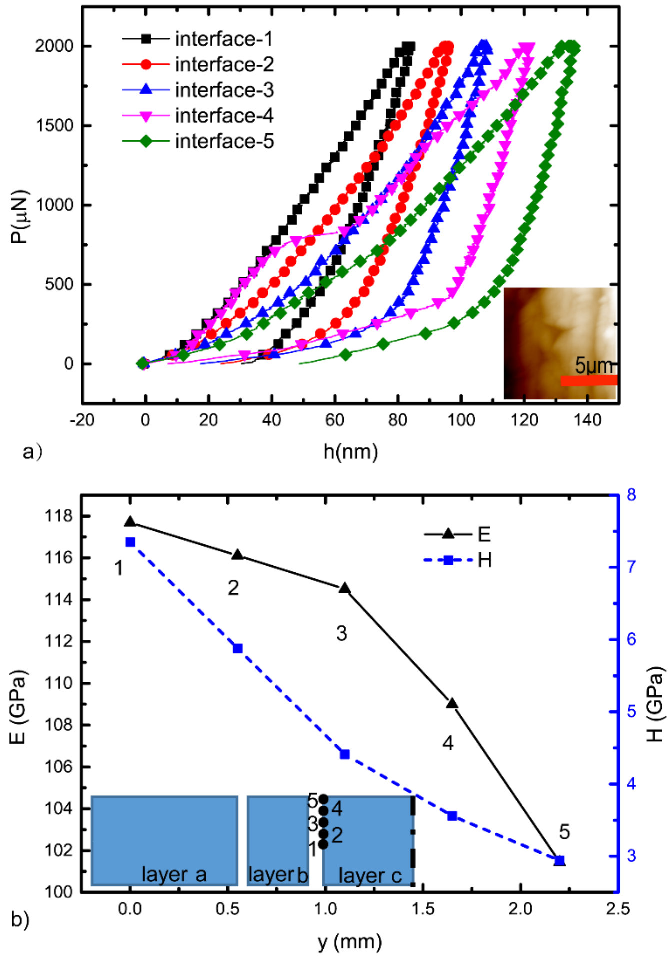

Fig.7 Nanoindentation experimental results of the interface of layer c (ZrO_2): a) load-displacement curve, b) modulus and hardness

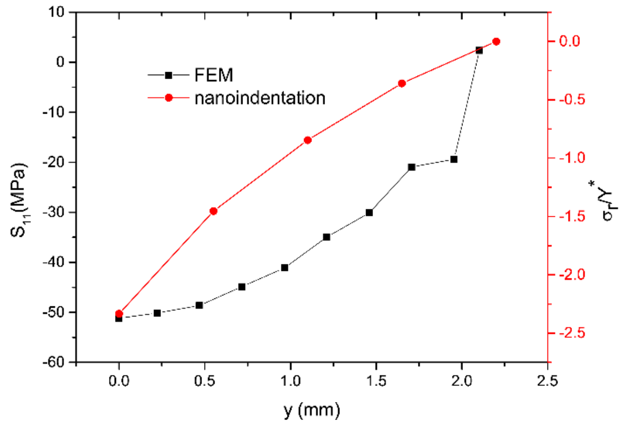

Fig.8 Comparison of residual stress of the interface of layer c determined by nanoindentation and FEM

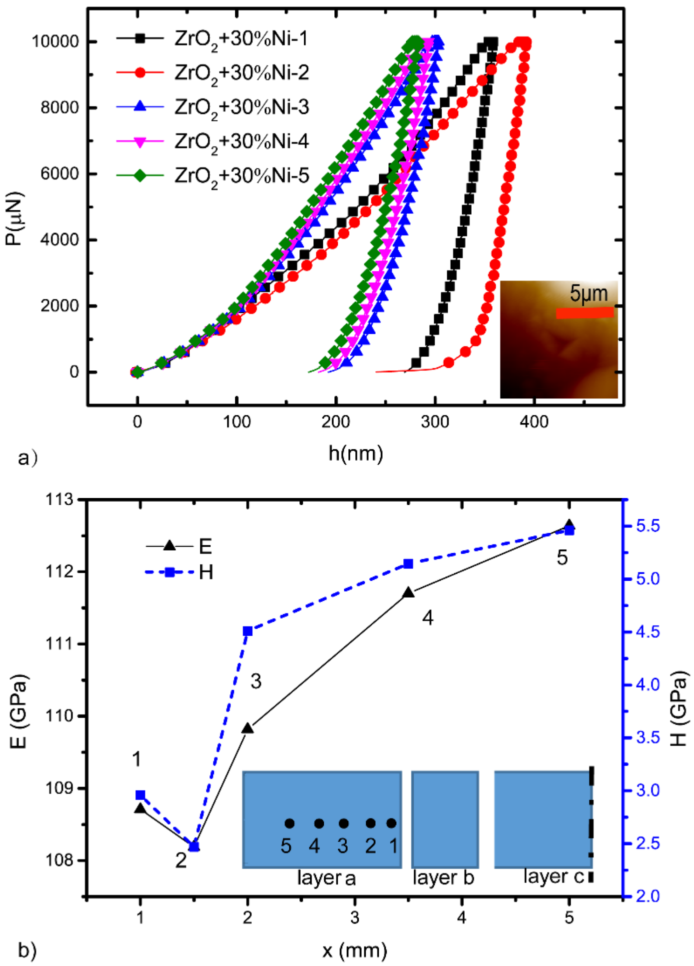

Fig.9 Nanoindentation experimental results of layer a (bearing load layer, ZrO_2+30 vol. %Ni): a) load-displacement curve, b) modulus and hardness

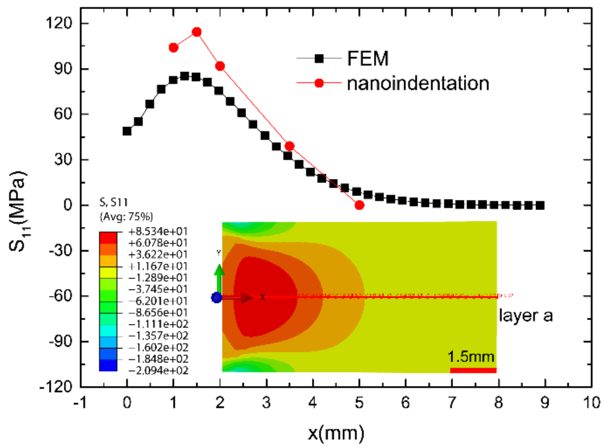

Fig.10 Comparison of residual stress of layer a determined by nanoindentation and FEM

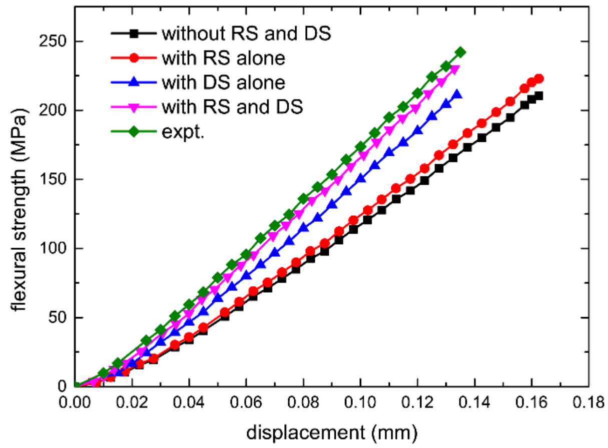

Fig.11 The flexural strength-displacement curves of the porous ZrO_2/(ZrO_2+Ni) ceramic-metal FGMs obtained by flexural test and FEM (RS-residual stress, DS-densification, expt.-experiment).

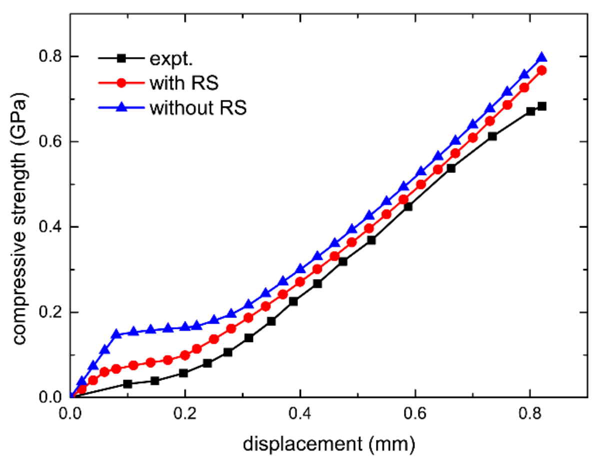

Fig.12 The compressive strength-displacement curves of the porous ZrO_2/(ZrO_2+Ni) ceramic-metal FGMs obtained by compressive test and FEM (RS-residual stress, expt.-experiment).